Optics & Laser Technology 154 (2022) 108340

Contents lists available at ScienceDirect

Optics and Laser Technology

journal homepage: www.elsevier.com/locate/optlastec

Full length article

Single polarization, narrow linewidth hybrid laser based on selective polarization mode feedback

Xichen Luo [a,b], Chao Chen [a,b,c,*], Yongqiang Ning [a,c], Jianwei Zhang [a], Jiaqi Chen [a], Xing Zhang [a], Lin Li [d], Hao Wu [a], Yinlin Zhou [a], Li Qin [a,c], Lijun Wang [a]

[a] State Key Laboratory of Luminescence and Applications, Changchun Institute of Optics, Fine Mechanics and Physics, Chinese Academy of Sciences, Changchun 130033, China
[b] Center of Materials Science and Optoelectronics Engineering, University of Chinese Academy of Sciences, Beijing 100049, China
[c] Xiongan Innovation Institute, Chinese Academy of Sciences, Xiongan 071800, China
[d] College of Physical and Electrical Engineering, Hainan Normal University, Haikou 571158, China

ARTICLE INFO

Keywords:
Narrow linewidth
Single polarization
Semiconductor laser
Hybrid integrated

ABSTRACT

We demonstrate a single polarization, narrow linewidth hybrid laser by using a semiconductor gain chip and a birefringence silica-on-silicon waveguide Bragg grating. The hybrid laser shows good linewidth and single polarization characteristics with the selective polarization mode feedback of high birefringence grating. The temperature phase modulation on the characteristics of the potentially lasing modes is displayed. In addition, the performances of different mode power, side mode suppress ratio, spectrum and linewidth during temperature tuning are characterized. We based on the rate equation method and the chirp factor reduction theory analysis the variation of laser linewidth with power and lasing wavelength. The best linewidth achieves 4.36 kHz and the best polarization extinction ratio is 38.6 dB. The output power in fiber is 6.58 mW.

1. Introduction

Narrow linewidth lasers not only play an important role in frontal science such as for optical clocks and gravitational wave detection [1–3], but are also widely used in other coherent optical systems including LiDAR and high precision spectrum detection [4–6]. In a coherent optical communication system, the receiver is sensitive to the linewidth, noise, and polarization of the signal, especially in a high order multilevel modulation system (16-QAM or more). The bit error rate (BER) of the receiver is directly related to the relative intensity noise (RIN) and the linewidth of the light source [7–9]. Furthermore, the local oscillation signal of the system requires a single polarization light source, but the input light usually uses a polarizer to achieve single polarization [10].

The linewidth of the laser is directly connected to the photon lifetime and it is closely related to the effective cavity length of laser. The linewidths of the distributed feedback (DFB) and the distributed Bragg reflector lasers are usually at the MHz or several hundred kHz level [11–13]. The best linewidth can achieve several tens of kHz [14], and the linewidth is limited by their relatively short cavity. Hence the common scheme of the narrow linewidth is based on the idea of extending the cavity length using external cavity. The linewidth of external Bragg grating or micro ring resonator hybrid laser can be easily suppressed to the kHz or the sub-kHz level [15–17], and both structures are the most attractive schemes to realize the narrow linewidth performance. Compared to the micro ring resonator, the structure of waveguide or fiber Bragg gratings are simpler and much easier to fabricate, which also means lower cost and simpler fabrication process. Grating based external cavity can greatly increase the effective cavity length of laser and suppress the linewidth with injection lock effect [18].

The measurement standard of a single polarization state is the polarization extinction ratio (PER), and the polarization stability of the laser is closely related to the PER. For narrow linewidth lasers operating in single polarization, most of the lasers with this output performance are fiber lasers with an active polarization mode control; the PER of these fiber lasers can achieve approximately 40 dB, and the linewidth is at the kHz level. The PER of a commercial narrow linewidth semiconductor laser is approximately 20 dB. Although a narrow linewidth semiconductor laser with a PER higher than 30 dB has been reported, its linewidth performance has not been clarified. Grating based external

* Corresponding author at: State Key Laboratory of Luminescence and Applications, Changchun Institute of Optics, Fine Mechanics and Physics, Chinese Academy of Sciences, Changchun 130033, China.
E-mail address: chenc@ciomp.ac.cn (C. Chen).

https://doi.org/10.1016/j.optlastec.2022.108340
Received 1 March 2022; Received in revised form 15 May 2022; Accepted 2 June 2022
Available online 9 June 2022

cavity lasers have a remarkable characteristic: mode hopping usually occurs as the current increases without phase modulation. As the bias current increases, the index changes due to the heating of gain chips, and the cavity phase would shift on the Bragg grating peak. The operation of the laser switches from a single longitudinal mode (SLM) to a multi-longitudinal mode (MLM) state unless the cavity phase cannot support SLM state [19–20]. Therefore, it is necessary to introduce phase modulation to achieve the alignment of the cavity phase and the grating peak. The common solution is to integrate the phase region on the grating or place a thermoelectric controller (TEC) on the heat sink of the gain chip. By adjusting the temperature of the phase region or TEC, a stable SLM state and a high side mode suppression ratio (SMSR) output can be achieved [21].

When the reflection of the grating is high enough and the backside of the gain chip (GC) is also coated with a high reflection (HR) film, it has the potential to achieve a lower linewidth. Because a higher reflection means a lower threshold current and stronger optical feedback, this is constructive to suppress spontaneous emission and enhance the photonic lifetime. However, there are some different characteristics in mode stability: more than one narrow mode in the cavity may have the potential to lase because the high reflection on the both sides leading to the small threshold gain. At the same time, the transmittance of different regions of the narrow band high reflection grating varies greatly, and the output power in different modes also varies substantially. Therefore, it is much more necessary to align the phase cavity with the grating spectrum.

In this paper, we demonstrate a single polarization narrow linewidth hybrid laser with a InP based GC and an external silica-on-silicon (SoS) waveguide Bragg grating (WBG). The output power reaches 6.53 mW, the best linewidth is 4.35 kHz, the PER of the laser reaches 38.6 dB and the RIN is lower than −158 dBc/Hz. On the basis of maintaining the kHz linewidth output and the low noise performance, our laser realizes the polarization mode stability compared with the active polarization mode-controlled fiber narrow linewidth laser. Furthermore, the effect of phase modulation on the output characteristic of a high reflection, narrow-band Bragg grating coupled to the gain chip is depicted, which shows some interesting results. The laser output power changes greatly at constant temperature, because of the sharp transmissivity change in the high reflection, narrow band WBG. It was also found that the laser can operate in three different modes in SLM state. Finally, the linewidths of the three modes of our laser are analyzed with the rate equation method and the chirp factor reduction theory.

2. Laser structure

The structure of the hybrid laser is shown in Fig. 1(a). It is composed of a 500 μm compressive strain quantum well GC to provide stronger TE mode gain and suppress TM mode amplified spontaneous emission. The gain region is relatively short; thus, the equivalent cavity is short and the mode competition is reduced. The length of the WBG is 5 mm and its structure is the same to [23]. The output of the WBG is coupled to a single channel fiber array. The WBG is a surface etched grating on the SoS platform, which utilizes the surface grating to enhance the shape birefringence and the high stress birefringence of the SoS platform itself to achieve large polarization mode splitting.

As shown in Fig. 1(b), the transmission spectrum of the WBG in circular polarization is measured by using a super-continuous spectrum laser light source (SuperK Compact, NKT Photonics, Inc.) and a optical spectrum analyzer (OSA, AQ6370D, Yokogawa). The wavelength splitting between the TE mode and the TM mode is 1.778 nm. In this way, the position of the TM mode is located at the position with lower gain to further suppress the TM mode. The back-side of the gain chip is coated with a high reflection film, which means that both sides of the equivalent laser cavity have high reflectivity. High reflectivity also means less terminate transmission, leading to relatively low output power. However, this scheme also enables more equivalent Fabry-Perot modes to be lased, even if the equivalent mode is located near the bottom of the Bragg resonance peak of the grating. Fig. 1(c) and (d) show the transmission spectrum when the laser is under a low bias current. The TM mode has been suppressed so only the TE mode exists in the spectrum. The black lines are caused by the minimum power detection of the optical spectrum analyzer. The bias current of Fig. 1 (d) is 16 mA, and the equivalent cavity modes can be seen in the figure.

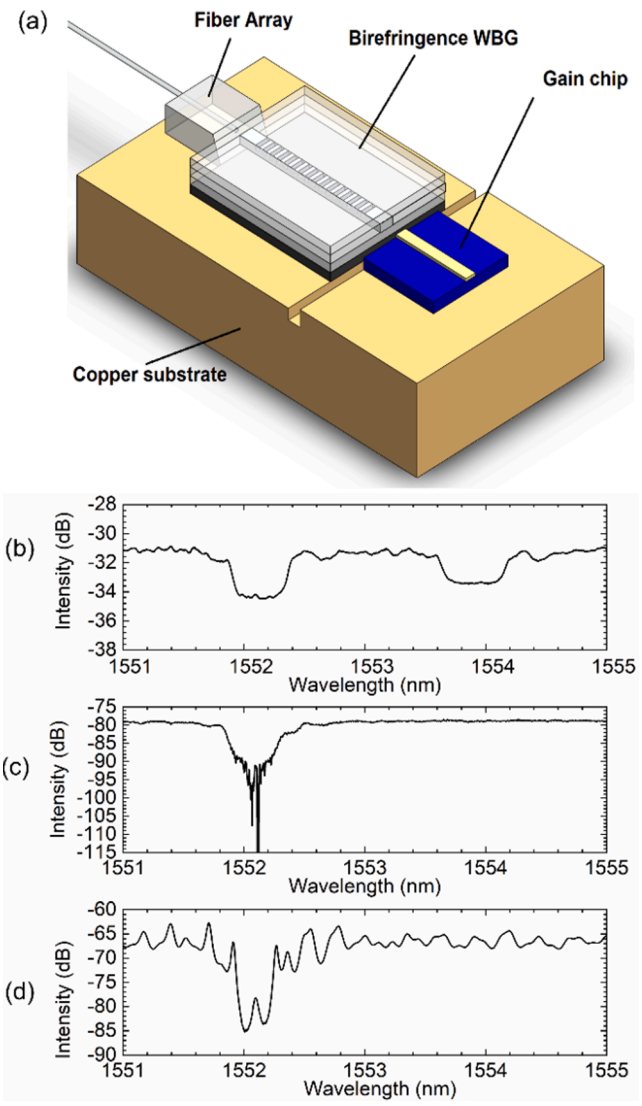

Fig. 1. (a) Schematic diagram of the hybrid laser (b) Transmission spectrum of the WBG in circular polarization. (c) Transmission spectrum under 16 mA. (d) Transmission spectrum under 22 mA.

3. Numerical analysis

We used the well-known rate equation to numerically analyses the linewidth of the hybrid laser [22]. The linewidth of the laser operated in single mode can be expressed as follows:

$$\Delta\nu_0 = \frac{R_{sp}}{P}(1+\alpha^2) \tag{1}$$

where the $\Delta\nu_0$ is the Fabry–Perot laser without external optical feedback,α is the linewidth enhancement factor, and R_{sp} is the spontaneous emission rate which is coupled to the lasing mode as follows:

$$R_{sp} = \beta_{sp}\eta_{sp}(An_r + BN + CN^2)N \tag{2}$$

β_{sp} and η_{sp} are the spontaneous emission factor and the spontaneous

quantum efficiency respectively. A, B and C represent the nonradiative, radiative and Auger recombination coefficients respectively.P is the photonic number, which is proportional to the difference between the injection current I_{inj} and the threshold current I_{th} as follows:

$$\mathrm{P} = \frac{I_{inj} - I_{\mathrm{th}}}{\mathrm{q}\Gamma \mathrm{v_g a}(\mathrm{N} - \mathrm{N_0})} \tag{3}$$

For our hybrid laser, the laser consists of an active region (gain chip) and a passive region (WBG). It would be convenient to consider this configuration as an equivalent F-P cavity laser with a complex wavelength dependent reflector, and its effective reflectivity R_{eff} of it is:

$$\mathrm{R_{eff}} = \frac{R_o + R_{OFB} + 2R_o R_{\mathrm{OFB}} \cos(\omega\tau_{\mathrm{e}})}{1 + R_o R_{OFB} + 2R_o R_{\mathrm{OFB}} \cos(\omega\tau_{\mathrm{e}})} \tag{4}$$

Where R_o is the anti-reflection terminates of the GC, $\tau_{\mathrm{e}} = 2\mathrm{nL_{ext}}/\mathrm{c}$ is the external round-trip delay (n is the refractive index of the WBG, L_{ext} is the length of the passive region), $R_{\mathrm{OFB}} = C_0{}^{*}R_g$ is the external feedback coupled to the GC, R_g is the power reflectivity of the WBG, which is defined as follows:

$$R_g = |R_{WBG}|^2 \tag{5}$$

$$R_{WBG} = \frac{-i\kappa}{\mu coth(\mu L_1) - (i\Delta\omega/v_g - \alpha_1)} \tag{6}$$

where κ is the coupling coefficient of the Bragg grating, v_g is the group velocity of the optical mode, α_1 is the waveguide attenuation, and $\Delta\omega$ is the laser angular frequency variable. Considering the phase change θ_{ref} induced by the WBG, $\mathrm{R_{eff}}$ is rewritten as follows:

$$\mathrm{R_{eff}} = \frac{R_o + R_{OFB} + 2R_o R_{\mathrm{OFB}} cos(\omega\tau_{\mathrm{e}} - \theta_{ref})}{1 + R_o R_{OFB} + 2R_o R_{\mathrm{OFB}} cos(\omega\tau_{\mathrm{e}} - \theta_{ref})} \tag{7}$$

Thus, the threshold current I_{th} with feedback by the WBG as follows:

$$I_{\mathrm{th}} = \mathrm{qVN_{th}}(A_{nr} + BN_{th} + CN_{th}) \tag{8}$$

where q is the electric charge, V is the active layer volume, B is the radiative recombination coefficient, A_{nr} is the nonradiative recombination coefficient and C represents the auger recombination process. $\mathrm{N_{th}}$ is the well-known carrier density equation at the threshold condition. With external optical feedback, $\mathrm{N_{th}}$ is defined as:

$$\mathrm{N_{th}} = N_0 + \frac{1}{\Gamma \mathrm{v_g} g \tau_{\mathrm{p}}} \tag{9}$$

N_0 is the transparency carrier density, Γ is the confinement factor, v_g is the group velocity, g represents the differential gain and τ_{p} denotes the photon lifetime. The feedback by the external filter can greatly enhanceτ_{p}, which is defined as follows:

$$\tau_{\mathrm{p}} = \frac{1}{\mathrm{v_g a_{tot}}} \tag{10}$$

a_{tot} is the total loss in the cavity loss composed of the internal cavity loss a_{int} and the mirror loss as follows:

$$a_{tot} = a_{int} + \frac{1}{2L_d} \ln \frac{1}{R_1 R_{reff}} \tag{11}$$

By solving the equations above, the theoretical linewidth and noise can be obtained. The simulated linewidth versus the bias current is shown in Fig. 2, and the linewidth approaches a minimum value with the reciprocal of the current in exponential form.

4. Experimental results and discussion

4.1. Constant temperature characteristic

Fig. 3(a) shows the power-current–voltage curves of the hybrid laser, and the curve of the power versus the current displays periodic

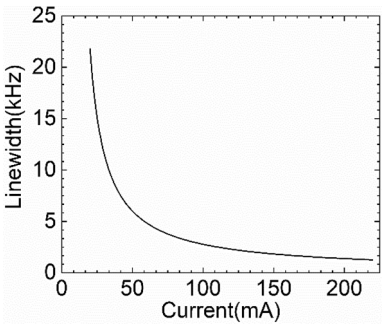

Fig. 2. The simulated linewidth as a function of current.

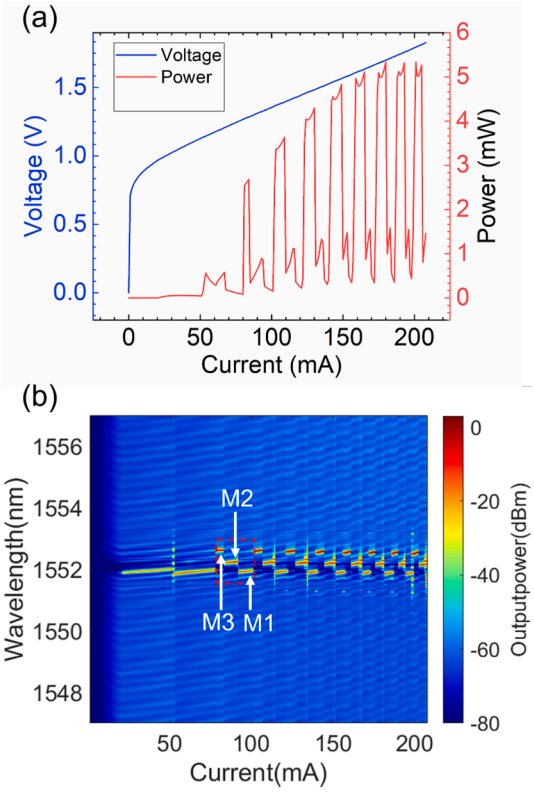

Fig. 3. The PIV curves and the optical spectra versus a current at a constant temperature.

vibration. The spectra plotted in the jet map also show this periodicity as seen in Fig. 3(b). The lasing wavelength of the hybrid laser shifts in the bandwidth of the Bragg grating peak as the gain chip is heating and the index of the chip changes to ensure that the cavity phase moves with the current. At a constant temperature, there are three adjacent modes (M1, M2 and M3 are named according to the order from short wavelength to long wavelength side) that could lase as shown in Fig. 3(b). There are three potential lasing modes because the free spectral range of the equivalent FP cavity is smaller than the bandwidth of the grating. Therefore, both terminates of the equivalent resonant cavity are high reflections at the wavelength corresponding to these three modes. The three modes have low threshold gain and the gain difference between them is small, leading to all three of them becoming the potential lasing mode. As the power curve shows, the three modes show some different characteristics: the mode located on the shorter side of the Bragg grating peak (M1) corresponds to the area where power decrease with bias current. In the case of M1 lasing, the wavelength moving to the longer side of WBG and the transmission decreases with the wavelength on the

shorter side of the Bragg resonance peak. M2 is located on the longer wavelength side of the WBG, but it is close to the center of the Bragg resonance peak. Therefore, the transmission is much lower than that of M3. M3 is the highest output power mode; it is on the far right of the Bragg resonance peak with high transmission and the highest output power.

4.2. Characteristics of the three lasing modes

By carefully adjusting the operating temperature of the hybrid laser, the alignment position between the laser cavity phase and the grating peak could be controlled, thus the gain difference between the lasing mode and the non-lasing modes can be adjusted and the lasing wavelength can be controlled to the ascertain mode. As the Fig. 4 shows, the lasing modes of the laser are controlled in three modes corresponding in Fig. 3. Each current point in the figure is adjusted to make the laser operate in the ascertained SLM state stably, all the current are above the threshold.

The lasing mode was first modulated to M1, and the features of this mode such as PIV curves, operating temperature, central wavelength, and SMSR are measured and are shown in Fig. 4 (a) to (e) respectively. In the adjustment process, increasing the bias current would cause the wavelength to move to the longer wavelength side, which is due to the plasma effect caused by the carrier injection. Therefore, the temperature tuning is needed to pull the cavity phase back to the best working position between the grating and the corresponding mode to ensure that the temperature decreases as the current increases in every single fluctuation period. However, the center of the lasing wavelength in Fig. 4(d) moves to the shorter wavelength side in every single period. This shows that the best alignment position between the grating and the mode changes in the temperature adjustment process. In addition to increasing the bias current, the work point gradually shifts to the shorter wavelength side.

At the same time, the SMSR in Fig. 4(e) also shows periodic characteristics with the adjustment of the current and the temperature. The SMSR decreases, which means that the gain difference between the other adjacent modes decreases. When the cavity phase cannot afford the current single mode operation, the tuning temperature should flash back to the higher temperature to find the best work point.

The output power of M3 is highest, because this mode is lasing at the place with the highest transmission of the grating compared to the other two modes. The highest output power achieves 6.53 mW at 208 mA.

The optical spectra of the corresponding three lasing modes plotted in the jet-map are shown in Fig. 5. All the points in the figure are operating in the SLM state, and the kicks in these figures are the points where the temperature flashes back to the higher temperature. The spectra on the right side show the operating condition in the optimal SMSR state of each mode. The corresponding currents for the three modes are 63 mA, 201 mA and 202 mA and the SMSR values are 50.28 dB, 49.04 dB and 58.05 dB. Moreover, the SMSR of mode M3 is excellent and the stability of M3 is also the best.

4.3. Polarization characteristics

To characterize the single polarization output characteristics of the laser, the PER is measured by a self-built PER measured system, which contains a linear polarization controller (Thorlabs, FBR-LPNIR), a photonic detector and a fixed bracket. By rotating the polarization controller in steps of 5° for a cycle and then recording the corresponding power, the normalized power diagram plotting in polar coordinates is shown in Fig. 6(a). The measured highest PER is 38.6 dB when the current is 160 mA and the lasing mode is controlled in the longest wavelength side; Such a high PER value means that the high birefringence WBG polarization mode selection works well. The PER at different currents is shown in Fig. 6(b), the PER above 160 mA decreases, which might be caused by power saturation of the gain chip, meaning that the power conversion efficiency of the TE mode decreases leading to a PER decrease.

4.4. Linewidth and RIN characteristics

We also measure the frequency noise power spectral density (FN-PSD) in different currents of the mode on the longest wavelength side and then calculated the linewidth of the laser with the β-separation line algorithm. This algorithm can be explained as follows: the β-separation line is defined as$S_{\delta\nu} = 8f\ln 2/\pi^2$, which divides the FN-PSD into two parts, and f is the frequency. The slow modulation area, which is$S_{\delta\nu} > 8f\ln 2/\pi^2$, has a notable influence on the value of linewidth. However, the fast modulation area, which is$S_{\delta\nu} < 8f\ln 2/\pi^2$, only contributes to the wings of the line shape of the laser [24–26]. By calculating the area M between FN-PSD and the β-separation line between the

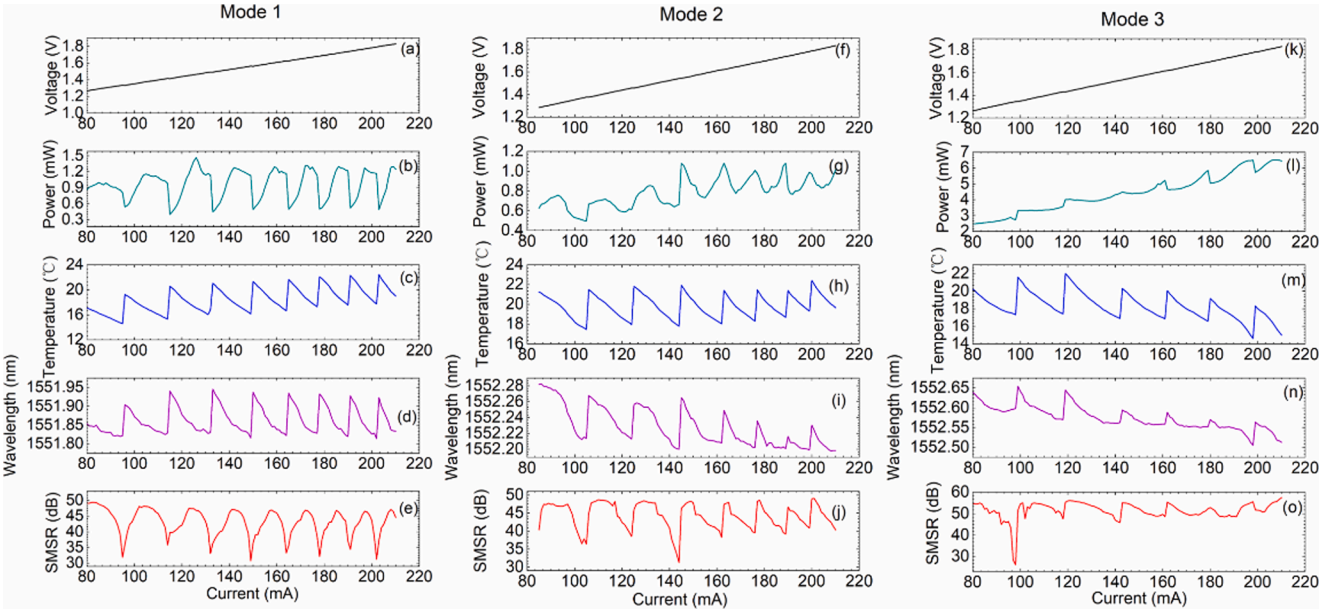

Fig. 4. PIV curves (a) and (b), operating temperature (c), center of the lasing wavelength (d) and side mode suppression ratio (e) in M1. The corresponding characteristics of M2 and M3 are shown in (f) to (j) and (k) to (o).

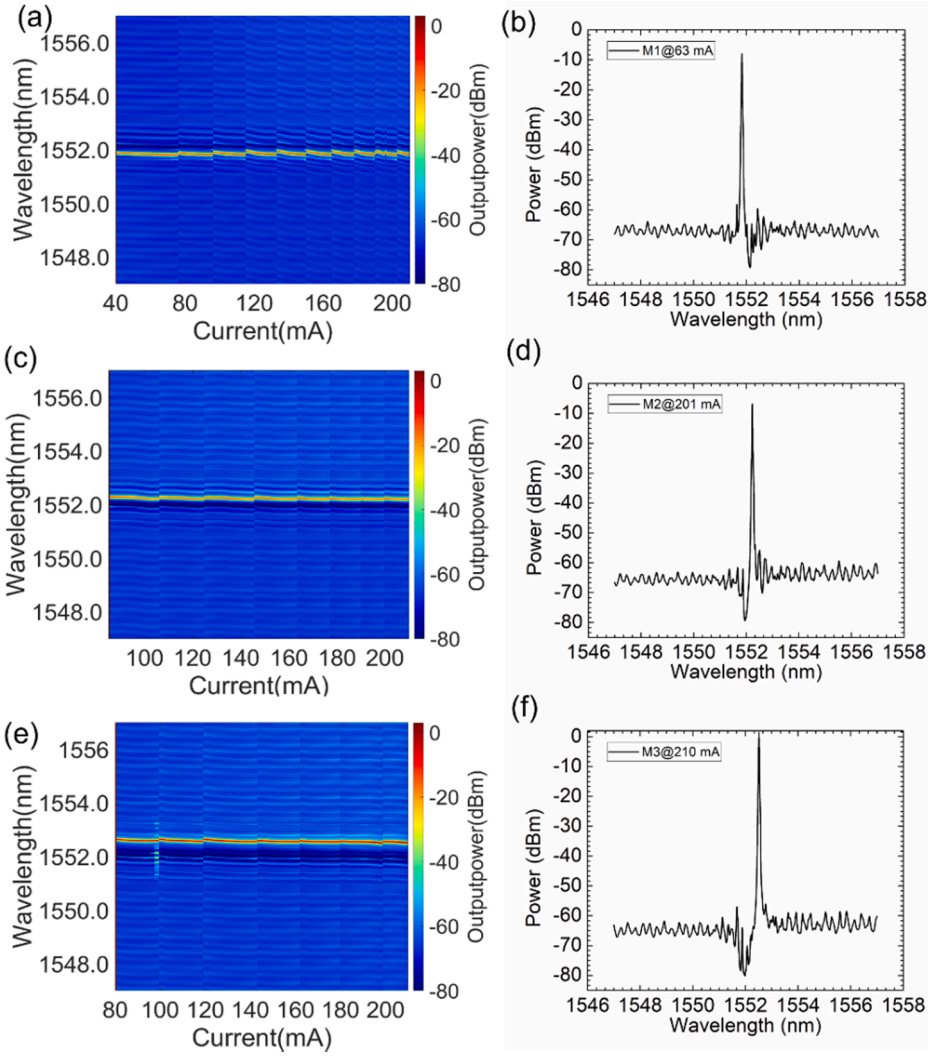

Fig. 5. The optical spectra of the three lasing modes plotted in the jet-map and the spectra of the three modes in the best SMSR.

isolation lines, the laser linewidth can be obtained by the formula as follows:

$$\Delta\nu = (8\mathrm{Mln}2)^{1/2} \tag{12}$$

The dynamic noise of our hybrid laser is measured based on the phase reconstruction principle. The laser output is injected into a 120-degree phase difference interferometer [27], and the differential phase information is measured. A schematic of the measurement system is shown in Fig. 7. The laser output is connected to a variable optical attenuator (VOA) to adjust to a suitable power. Then the light is divided into two parts by the circulator: one part is connected to the photodetector as a reference, and the other part is connected to 3 × 3 coupler. Output ports 1, and 2 of the coupler are reflected back to the coupler by Faraday mirrors and mutually interfere with a delay fiber. While output port 3 is empty, the three outputs of the coupler have equal amplitudes and phase difference of 120°. The output data are collected to an analog card, and then used polynomial linear fitting to investigate the frequency/phase characteristics that deviate from the linear sweep. Then, the FN-PSD of the hybrid laser within a specific time is obtained by demodulating the measured phase information.

Fig. 8 shows the narrowest linewidth of the laser and the bias current is 155 mA. The blue line is the measured FN-PSD and the grey line is the β-separation line. The minimum integration linewidth in Fig. 8(a) is 4.36 kHz, the white noise platform is 1140 Hz^2/Hz@1MHz and the corresponding Lorentzian linewidth is approximately 3.58 kHz. The integration linewidth is slightly higher than Lorentzian linewidth because the fast modulation areas contribute to the line shape.

The linewidths of the other two modes on the shorter wavelength side has also been measured, and they are 58.63 kHz and 60.18 kHz. Compared with M3, these linewidth values are approximately 15 times larger. The linewidth difference of lasing at various positions of grating can be analyzed by the chirp reduction factor F = 1 + A + B, and the linewidth of the free-running laser is suppressed by $1/F^2$ with the feedback of WBG self-injection mode locking [28–30], where:

$$A = \frac{1}{\tau_{GC}} Re\left\{ i \frac{d}{d\omega} \ln R_{eff}(\omega) \right\} \tag{13}$$

$$B = \frac{\alpha}{\tau_{GC}} Im\left\{ i \frac{d}{d\omega} \ln R_{eff}(\omega) \right\} \tag{14}$$

The reason for the chirp is that the phase changes with the carrier concentration, which is caused by spontaneous emission and other factors. Reducing the chirp can narrow the linewidth. For the external cavity negative feedback laser, parameter A represents the improvement of the effective cavity length by the extended cavity, which enhances the photon lifetime and suppresses the intrinsic linewidth. Parameter B represents the influence of the negative feedback caused by WBG self-injection locking. The process of negative feedback is usually as follows, on the long wavelength side of the grating:

a. Operating wavelength detuning to the short (long) side.

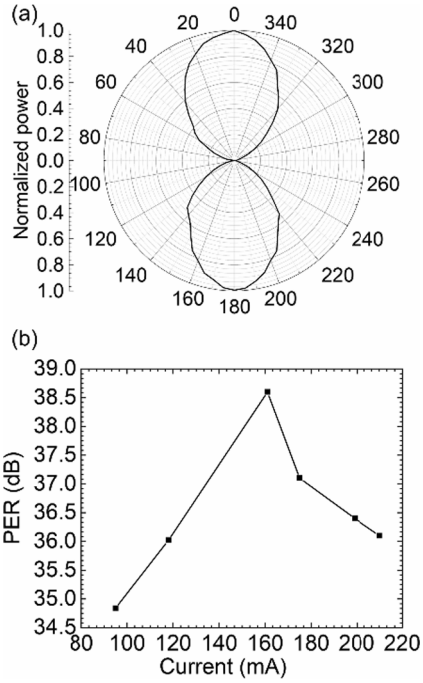

Fig. 6. The normalized power versus angle (a) and the PER value operated in single mode at different currents.

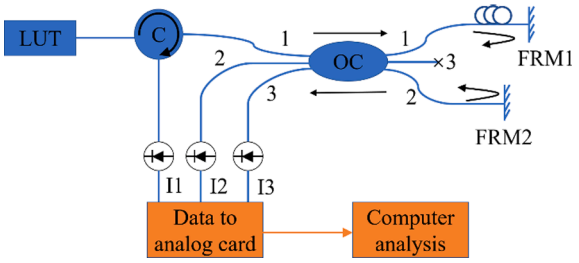

Fig. 7. Schematic of the measurement system.

b. The amplitude corresponding to the effective reflectivity increases (decreases).

c. The light field reflected by the WBG increases (decreases), and the photon density in the cavity increases (decreases).

d. The carrier density is reduced (increased) due to spontaneous emission.

e. As a result of the carrier plasma effect, the wavelength shifts to the long (short) side.

After the above process, the lasing wavelength can be stabilized. As a result, the negative feedback effect stabilizes the frequency and reduces the phase fluctuation, leading to the suppression of the linewidth and the RIN.

$\tau_{GC} = 2n_{eff}L_a/c$ is the delay time of the optical mode propagation in the gain chip for one loop, and n_{eff} is the effective index of GC. The calculated F and the corresponding results are shown in Fig. 9. The shape of R_{eff} is derived from the superposition of the grating and the equivalent FP cavity mode. Corresponding to the positions of the three modes within the grating bandwidth, the value of F is large at every valley ofR_{eff}, which is close to the position with the highest transmittance of each cavity mode, meaning that lower optical confinement. The maximum values of F are 9.04, 9.21 and 43.52 respectively, which causes an approximately 25-fold linewidth reduction difference. The reason for the difference from the actual linewidth might be that the lasing wavelength of M3 is not at the maximum of F, and the actual

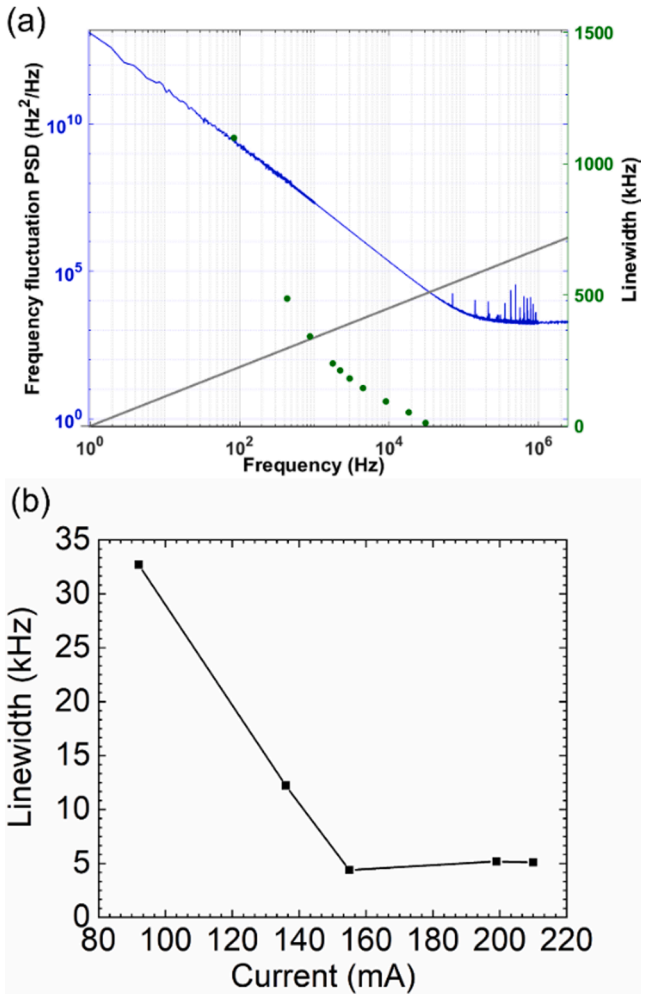

Fig. 8. (a)Measured FN-PSD spectrum with narrowest linewidth and (b) measured linewidth under different currents.

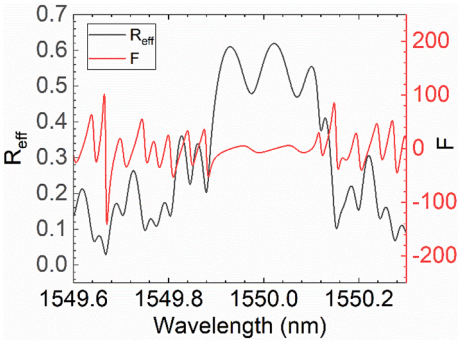

Fig. 9. Calculated R_{eff} and the F factor.

linewidth difference is smaller than expected. One possible reason for this is that the actual lasing position is not at the position of the maximum F value of each mode, but the B value changes considerably with the wavelength r, detuning around the energy gap. That is, the actual F value of the M3 is smaller than expected.

As shown in Fig. 8(b), the laser linewidth under different currents (95 mA, 115 mA, 135 mA, 155 mA, 175 mA, 195 mA and 210 mA corresponding to the period in Fig. 4. The linewidth is decreases considerably in the initial current range, showing the trend of that is consistent with the simulation results in Fig. 2. Above 155 mA, the

linewidth has little difference or even increases slightly. This is because the power saturation of the gain chip increases the noise characteristic of the laser, and these phenomena can also be observed in the RIN test..

The RIN of the laser is measured by a photonic detector, an RF amplifier, and an electric spectrum analyzer, which are used to measure and analyze the laser frequency signal. Fig. 10 shows the results corresponding to the current in Fig. 7(b). In the range of 95 mA to 155 mA, the RIN of the laser decreases with the current, and the lowest RIN reaches −158 dBc/Hz@1MHz. However, the RIN is larger when the current at the range of 175 mA to 210 mA, where the power saturation occurs, as shown by the PIV curves in Fig. 3.

4.5. Frequency and long-term output power stability

To further demonstrate the stable mode operation of our laser, we measured and calculated the Allan deviations of the three modes according to the frequency noise power spectrum density as shown in the Fig. 11(a), all the operation currents are 155 mA and then the lasing mode is adjusted to the three modes respectively according to the Fig. 4. The lowest Allan deviation of the M3 reaches 1.531×10^{-10} at 1 MHz, showing excellent transient power stability. The transient stability is due to the strong negative feedback effect away from the resonant center of the WBG. However, the Allan deviations of the other two modes are 3.45×10^{-10} and 4.951×10^{-10} respectively, so M3 is the most stable mode according to the Allan deviations. Furthermore, the long-term output power of the three modes has also been measured. The laser operates in M3, the monitoring time is 1 h and the sampling interval is 1 s. As shown in Fig. 11(b), the measured average power of M3 is 4.623 mW, and the standard deviation of power fluctuation is 0.0065. The standard deviations of the other two modes are 0.0089 and 0.0082 respectively. Therefore, it can be seen that m3 has more stable long-term power output stability.

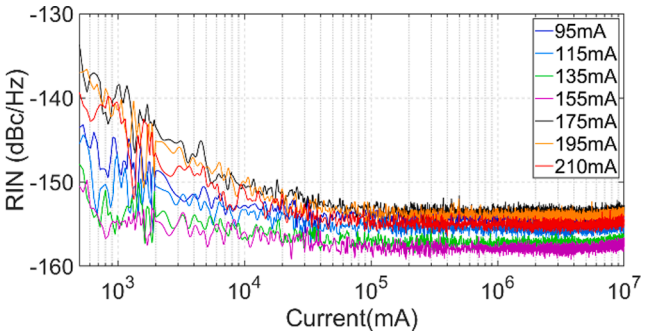

Fig. 10. Measured RIN spectrum under different current (from 95 mA to 210 mA).

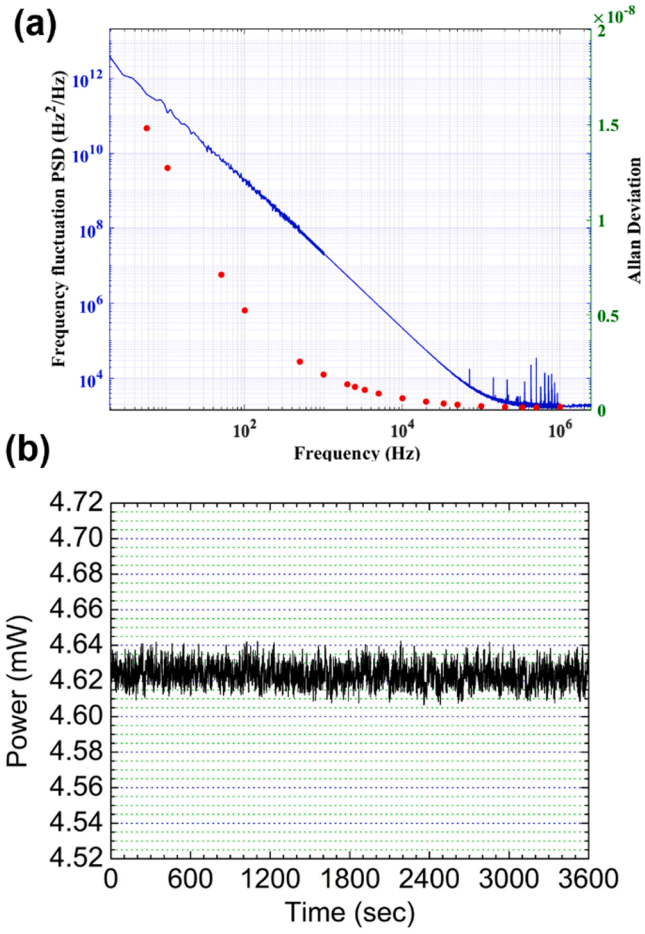

Fig. 11. (a) Calculated Allan deviations of M3 (b) long-term output power stability of M3.

5. Conclusions

To summarize, we demonstrate a hybrid narrow linewidth semiconductor laser with single polarization. The narrowest linewidth achieves 4.36 kHz and the PER achieves 38.4 dB. Based on rate equation of the hybrid laser, we numerically analyze the linewidth characteristic and its trend is consistent with the experimental results. The temperature phase modulation to the three adjacent modes contained in the bandwidth of the WBG is also demonstrated. The adjustment of the temperature can align the adjacent cavity mode with the grating, and the gain between cavity modes can be controlled to lase the determined mode. Finally, the PER, linewidth and the RIN are also measured at different currents corresponding to every single current period. The PER value achieves 38.6 dB, the narrowest linewidth achieves 4.36 kHz and the lowest RIN is −158 dBc/Hz, which shows excellent single polarization, narrow linewidth and low relative inensity noise performances. The results also show that the power saturation effect has a considerable influence on three mode characteristics, and these three performances are degraded in varying degrees after power saturation.

CRediT authorship contribution statement

Xichen Luo: Methodology, Software, Investigation, Writing – original draft. **Chao Chen:** Conceptualization, Methodology, Validation, Writing – original draft, Writing – review & editing. **Yongqiang Ning:** Supervision. **Jianwei Zhang:** Data curation. **Jiaqi Chen:** Formal analysis. **Xing Zhang:** Visualization. **Lin Li:** Formal analysis. **Hao Wu:** Visualization. **Yinlin Zhou:** Visualization. **Li Qin:** Project administration. **Lijun Wang:** Resources.

Declaration of Competing Interest

The authors declare that they have no known competing financial interests or personal relationships that could have appeared to influence the work reported in this paper.

Acknowledgment

This work is supported by the National Natural Science Foundation of China (61874119, 61727822, 11774343, 51672264, 62174046), Science and Technology Development Project of Jilin Province (20200401006GX), and Finance Science and Technology Project of Hainan Province (ZDYF2020217).

References

[1] M. Schioppo, R.C. Brown, W.F. McGrew, N. Hinkley, R.J. Fasano, K. Beloy, T. H. Yoon, G. Milani, D. Nicolodi, J.A. Sherman, N.B. Phillips, C.W. Oates, A. D. Ludlow, Ultrastable optical clock with two cold-atom ensembles, Nature Photon. 11 (1) (2017) 48–52.

[2] K. Numata, A. Yu, J. Camp, M. Krainak, Laser system development for gravitational-wave interferometry in space, Proc. SPIE (2018) 10511D.

[3] Z.L. Newman, V. Maurice, T. Drake, J.R. Stone, T.C. Briles, D.T. Spencer, C. Fredrick, Q. Li, D. Westly, B.R. Ilic, B. Shen, M.-G. Suh, K.Y. Yang, C. Johnson, D. M.S. Johnson, L. Hollberg, K.J. Vahala, K. Srinivasan, S.A. Diddams, J. Kitching, S. B. Papp, M.T. Hummon, Architecture for the photonic integration of an optical atomic clock, Optica 6 (5) (2019) 680, https://doi.org/10.1364/OPTICA.6.000680.

[4] J. Labaziewicz, P. Richerme, K.R. Brown, I.L. Chuang, K. Hayasaka, Compact, filtered diode laser system for precision spectroscopy, Opt. Lett. 32 (5) (2007) 572, https://doi.org/10.1364/OL.32.000572.

[5] L. Tang, H. Jia, S. Shao, S. Yang, H. Chen, M. Chen, Hybrid integrated low-noise linear chirp frequency-modulated continuous-wave laser source based on self-injection to an external cavity, Photon. Res. 9 (10) (2021) 1948, https://doi.org/10.1364/PRJ.428837.

[6] Y.-H. Lai, M.-G. Suh, Y.-K. Lu, B. Shen, Q.-F. Yang, H. Wang, J. Li, S.H. Lee, K. Y. Yang, K. Vahala, Earth rotation measured by a chip-scale ring laser gyroscope, Nature Photon. 14 (6) (2020) 345–349.

[7] E. Fujita, Y. Mashiko, S. Asaya, M. Musha, M. Tokurakawa, High power narrow-linewidth linearly-polarized 1610 nm Er: Yb all-fiber MOPA, Opt. Express 24 (23) (2016) 26255, https://doi.org/10.1364/OE.24.026255.

[8] M. Faugeron, M. Tran, F. Lelarge, M. Chtioui, Y. Robert, E. Vinet, A. Enard, J. Jacquet, F.V. Dijk, High-Power, Low RIN 1.55-um Directly Modulated DFB Lasers for Analog Signal Transmission, Photon. Technol. Lett. 24 (2012) 116–118.

[9] M. Seimetz, Laser Linewidth Limitations for Optical Systems with High-Order Modulation Employing Feed Forward Digital Carrier Phase Estimation, in OFC/NFOEC , 1-3 (OTuM2) (2008).

[10] K. Endo, Y. Hashimoto, T. Tanaka, T. Takamichi, K. Fukuchi, M. Toyoshima, Y. Takayama, Development and evaluation of a digital signal processing for single polarization QPSK modulation format, Proc SPIE (2012) 82460A.

[11] B. Janjua, M.L. Iu, Z. Yan, P. Charles, E. Chen, A.S. Helmy, Distributed feedback lasers using surface gratings in Bragg waveguides, Opt. Lett. 46 (15) (2021) 3689, https://doi.org/10.1364/OL.431292.

[12] P. Doussiere, C.-L. Shieh, S. DeMars, K. Dzurko, Very high-power 1310nm InP single mode distributed feed back laser diode with reduced linewidth, Proc SPIE (2007) 6485G.

[13] E.D. Gaetano, M. Sorel, Design of chirped-coupling sidewall Bragg gratings for narrow linewidth distributed feedback lasers, Opt. Lett. 44 (7) (2019) 1642, https://doi.org/10.1364/OL.44.001642.

[14] S. Spiessberger, M. Schiemangk, A. Wicht, H. Wenzel, O. Brox, G. Erbert, Narrow Linewidth DFB Lasers Emitting Near a Wavelength of 1064 nm, J. Lightw. Technol. 28 (17) (2010) 2611–2616.

[15] Y.u. Li, Y. Zhang, H. Chen, S. Yang, M. Chen, Tunable Self-Injected Fabry-Perot Laser Diode Coupled to an External High-Q Si3N4 /SiO2 Microring Resonator, J. Lightw. Technol. 36 (16) (2018) 3269–3274.

[16] D. Huang, M.A. Tran, J. Guo, J. Peters, T. Komljenovic, A. Malik, P.A. Morton, J. E. Bowers, High-power sub-kHz linewidth lasers fully integrated on silicon, Optica 6 (6) (2019) 745, https://doi.org/10.1364/OPTICA.6.000745.

[17] Z. Wang, K. Van Gasse, V. Moskalenko, S. Latkowski, E. Bente, B. Kuyken, G. Roelkens, A III-V-on-Si ultra-dense comb laser, Light: Sci, Appl. 6 (2017) e16260.

[18] Y. Zhang, Y. Zhang, Q. Zhao, C. Li, C. Yang, Z. Feng, H. Deng, E. Zhou, X. Xu, K.K. Y. Wong, Z. Yang, S. Xu, Ultra-narrow linewidth full C-band tunable single-frequency linear-polarization fiber laser, Opt. Express 24 (23) (2016) 26209, https://doi.org/10.1364/OE.24.026209.

[19] P.A. Morton, M.J. Morton, High-Power, Ultra-Low Noise Hybrid Lasers for Microwave Photonics and Optical Sensing, J. Lightw. Technol. 36 (21) (2018) 5048–5057.

[20] Y. Guo, R. Zhao, G. Zhou, L. Lu, A. Stroganov, M.S. Nisar, J. Chen, L. Zhou, Thermally Tuned High-Performance III-V/Si3N4 External Cavity Laser, IEEE Photonics J. 13 (2021) 1–13.

[21] M. Happach, D. De Felipe, V.N. Friedhoff, M. Kresse, G. Irmscher, M. Kleinert, C. Zawadzki, W. Rehbein, W. Brinker, M. Mohrle, N. Keil, W. Hofmann, M. Schell, Influence of Integrated Optical Feedback on Tunable Lasers, IEEE J. Quantum Electron. 56 (1) (2020) 1–7.

[22] H.K. Hisham, A.F. Abas, G.A. Mahdiraji, M.A. Mahdi, A.S.M. Noor, Relative Intensity Noise Reduction by Optimizing Fiber Grating Fabry-Perot Laser Parameters, IEEE J. Quantum Electron. 48 (3) (2012) 375–383.

[23] X.-C. Luo, C. Chen, L.i. Qin, X. Zhang, Y.-y. Chen, B. Wang, L. Liang, P. Jia, Y.-Q. Ning, L.-J. Wang, High-birefringence waveguide Bragg gratings fabricated in a silica-on-silicon platform with displacement Talbot lithography, Opt. Mater. Express 10 (10) (2020) 2406, https://doi.org/10.1364/OME.402937.

[24] N. Bucalovic, V. Dolgovskiy, C. Schori, P. Thomann, G. Di Domenico, S. Schilt, Experimental validation of a simple approximation to determine the linewidth of a laser from its frequency noise spectrum, Appl. Opt. 51 (20) (2012) 4582, https://doi.org/10.1364/AO.51.004582.

[25] Q. Zhou, J. Qin, W. Xie, Z. Liu, Y. Tong, Y.i. Dong, W. Hu, Power-area method to precisely estimate laser linewidth from its frequency-noise spectrum, Appl. Opt. 54 (28) (2015) 8282, https://doi.org/10.1364/AO.54.008282.

[26] G. Di Domenico, S. Schilt, P. Thomann, Simple approach to the relation between laser frequency noise and laser line shape, Appl. Opt. 49 (25) (2010) 4801, https://doi.org/10.1364/AO.49.004801.

[27] X.i. Zhang, F. Yang, Z. Feng, F. Wei, H. Cai, R. Qu, Narrow-linewidth swept laser phase reconstruction and noise measurement technology and its applications, Opt. Express. 26 (25) (2018) 32958, https://doi.org/10.1364/OE.26.032958.

[28] R. Kazarinov, C. Henry, The relation of line narrowing and chirp reduction resulting from the coupling of a semiconductor laser to passive resonator, IEEE J. Quantum Electron. 23 (9) (1987) 1401–1409.

[29] G.P. Agrawal, C.H. Henry, Modulation performance of a semiconductor laser coupled to an external high-Q resonator, IEEE J. Quantum Electron. 24 (2) (1988) 134–142.

[30] T. Komljenovic, J. Bowers, Monolithically Integrated High-Q Rings for Narrow Linewidth Widely Tunable Lasers, J. Quantum Electron. 51 (2015) 1–10.